Available online at www.sciencedirect.com
ScienceDirect
Solar Energy 81 (2007) 254–267
SOLAR ENERGY
www.elsevier.com/locate/solener

Empirical validation of models to compute solar irradiance on inclined surfaces for building energy simulation

P.G. Loutzenhiser [a,b,*], H. Manz [a], C. Felsmann [c], P.A. Strachan [d], T. Frank [a], G.M. Maxwell [b]

[a] Swiss Federal Laboratories for Materials Testing and Research (EMPA), Laboratory for Applied Physics in Buildings, CH-8600 Duebendorf, Switzerland
[b] Iowa State University, Department of Mechanical Engineering, Ames, IA 50011, USA
[c] Technical University of Dresden, Institute of Thermodynamics and Building Systems Engineering, D-01062 Dresden, Germany
[d] University of Strathclyde, Department of Mechanical Engineering, ESRU, Glasgow G1 1XJ, Scotland, UK

Received 27 July 2005; received in revised form 28 February 2006; accepted 3 March 2006
Available online 12 May 2006

Communicated by: Associate Editor David Renne

Abstract

Accurately computing solar irradiance on external facades is a prerequisite for reliably predicting thermal behavior and cooling loads of buildings. Validation of radiation models and algorithms implemented in building energy simulation codes is an essential endeavor for evaluating solar gain models. Seven solar radiation models implemented in four building energy simulation codes were investigated: (1) isotropic sky, (2) Klucher, (3) Hay–Davies, (4) Reindl, (5) Muneer, (6) 1987 Perez, and (7) 1990 Perez models. The building energy simulation codes included: EnergyPlus, DOE-2.1E, TRNSYS-TUD, and ESP-r. Solar radiation data from two 25 days periods in October and March/April, which included diverse atmospheric conditions and solar altitudes, measured on the EMPA campus in a suburban area in Duebendorf, Switzerland, were used for validation purposes. Two of the three measured components of solar irradiances – global horizontal, diffuse horizontal and direct-normal – were used as inputs for calculating global irradiance on a south-west façade. Numerous statistical parameters were employed to analyze hourly measured and predicted global vertical irradiances. Mean absolute differences for both periods were found to be: (1) 13.7% and 14.9% for the isotropic sky model, (2) 9.1% for the Hay–Davies model, (3) 9.4% for the Reindl model, (4) 7.6% for the Muneer model, (5) 13.2% for the Klucher model, (6) 9.0%, 7.7%, 6.6%, and 7.1% for the 1990 Perez models, and (7) 7.9% for the 1987 Perez model. Detailed sensitivity analyses using Monte Carlo and fitted effects for *N*-way factorial analyses were applied to assess how uncertainties in input parameters propagated through one of the building energy simulation codes and impacted the output parameter. The implications of deviations in computed solar irradiances on predicted thermal behavior and cooling load of buildings are discussed.

Keywords: Solar radiation models; Empirical validation; Building energy simulation; Uncertainty analysis

1. Introduction

In the 21st century, engineers and architects are relying increasingly on building energy simulation codes to design more energy-efficient buildings. One of the common traits found in new commercial buildings across Europe and the United States is construction with large glazed façades. Accurate modeling of the impact of solar gains through glazing is imperative especially when simulating the

* Corresponding author. Address: Swiss Federal Laboratories for Materials Testing and Research (EMPA), Laboratory for Applied Physics in Buildings, CH-8600 Duebendorf, Switzerland. Tel.: +41 44 823 43 78; fax: +41 44 823 40 09.
E-mail address: peter.loutzenhiser@empa.ch (P.G. Loutzenhiser).

0038-092X/$ - see front matter © 2006 Elsevier Ltd. All rights reserved.
doi:10.1016/j.solener.2006.03.009

Nomenclature

A	anisotropic index, –
B	radiation distribution index, –
a, b	terms that account for the incident angle on the sloped surface, –
D	hourly difference between experimental and predicted values for a given array, W/m^2
D_{max}	maximum difference between experimental and predicted values for a given array, W/m^2
D_{min}	minimum difference between experimental and predicted values for a given array, W/m^2
D_{rms}	root mean squared difference between experimental and predicted values for a given array, W/m^2
$D_{95\%}$	ninety-fifth percentile of the differences between experimental and predicted values for a given array, W/m^2
d	estimated error quantity provided by the manufacturer, units vary
F_1	circumsolar coefficient, –
F_2	brightness coefficient, –
F'	clearness index, –
f_{11}, f_{12}, f_{13}, f_{21}, f_{22}, f_{23}	statistically derived coefficients derived from empirical data for specific locations as a function of ε, –
I_{bn}	direct-normal solar irradiance, W/m^2
I_h	global horizontal solar irradiance, W/m^2
$I_{h,b}$	direct-normal component of solar irradiance on the horizontal surface, W/m^2
$I_{h,d}$	global diffuse horizontal solar irradiance, W/m^2
I_{on}	direct extraterrestrial normal irradiance, W/m^2
I_T	solar irradiance on the tilted surface, W/m^2
$I_{T,b}$	direct-normal (beam) component of solar irradiance on the tilted surface, W/m^2
$I_{T,d}$	diffuse component of solar irradiance on the tilted surface, W/m^2
$I_{T,d,iso}$	isotropic diffuse component of solar irradiance on the tilted surface, W/m^2
$I_{T,d,cs}$	circumsolar diffuse component of solar irradiance on the tilted surface, W/m^2
$I_{T,d,hb}$	horizontal brightening diffuse component of solar irradiance on the tilted surface, W/m^2
$I_{T,d,g}$	reflected ground diffuse component of solar irradiance on the tilted surface, W/m^2
i, j	indices the n-factorial study the represent different levels of input parameters, –
m	relative optical air mass, –
OU	overall uncertainty at each hour for the experiment and EnergyPlus for 95% credible limits, W/m^2
$\overline{\mathrm{OU}}$	average overall uncertainty calculated for 95% credible limits, W/m^2
s	sample standard deviation, W/m^2
R_b	variable geometric factor which is a ratio of tilted and horizontal solar beam irradiance
u	is the individual or combined effects from the n-factorial study, W/m^2
TF	tilt factor, –
UR	computed uncertainty ratio at each hour for comparing overall performance of a given model, –
$\overline{\mathrm{UR}}$	average uncertainty ratio, –
UR_{max}	maximum uncertainty ratio, –
UR_{min}	minimum uncertainty ratio, –
$\bar{x}$	arithmetic mean for a given array of data, W/m^2
x_{min}	minimum quantity for a given array of data, W/m^2
x_{max}	maximum quantity for a given array of data, W/m^2

Greek symbols

α	absorptance, %
α_n	normal absorptance, %
α_s	solar altitude angle, °
β	surface tilt angle from horizon, °
Δ	sky condition parameter for brightness, –
ε	sky condition parameter for clearness, –
ϕ_b	building azimuth, °
θ	incident angle of the surface, °
θ_z	zenith angle,°
ξ	input parameter n-way factorial, units vary
ρ	hemispherical-hemispherical ground reflectance, –
σ	standard deviation n-way factorial, units vary

thermal behavior of these buildings. Empirical validations of solar gain models are therefore an important and necessary endeavor to provide confidence to developers and modelers that their respective algorithms simulate reality.

A preliminary step in assessing the performance of the solar gain models is to examine and empirically validate models that compute irradiance on exterior surfaces. Various radiation models for inclined surfaces have been proposed – some of which have been implemented in building energy simulation codes – which include isotropic models (Hottel and Woertz, 1942 as cited by Duffie and Beckman, 1991; Liu and Jordan, 1960; Badescu, 2002), anisotropic models (Perez et al., 1990, 1986; Gueymard, 1987; Robledo and Soler, 2002; Li et al., 2002; Olmo et al., 1999; Klucher, 1979; Muneer, 1997) and models for a clear sky (Robledo and Soler, 2002). Comparisons and modifications to these models and their applications to specific regions in the world have also been undertaken (Behr, 1997; Remund et al., 1998).

In all empirical validations, accounting for uncertainties in the experiment and input parameters is paramount. Sensitivity analysis is a well-established technique in computer simulations (Saltelli et al., 2004; Saltelli et al., 2000; Santner et al., 2003) and has been implemented in building energy simulation codes (Macdonald and Strachan, 2001) and empirical validations (Mara et al., 2001; Aude et al., 2000; Fürbringer and Roulet, 1999; Fürbringer and Roulet, 1995; Lomas and Eppel, 1992) for many years. A thorough methodology for sensitivity analysis for calculations, correlation analysis, principle component analysis, and implementation in the framework of empirical validations in IEA-SHC Task 22 are described by Palomo del Barrio and Guyon (2003, 2004).

In the context of the International Energy Agency's (IEA) SHC Task 34/ECBCS Annex 43 Subtask C, a series of empirical validations is being performed in a test cell to assess the accuracy of solar gain models in building energy simulation codes with/without shading devices and frames. A thorough description of the proposed suite of experiments, description of the cell, rigorous evaluation of the cell thermophysical properties and thermal bridges, and a methodology for examining results are reported by Manz et al. (in press).

In virtually all building energy simulation applications, solar radiation must be calculated on tilted surfaces. These calculations are driven by solar irradiation inputs or appropriate correction factors and clear sky models. While the horizontal irradiation is virtually always measured, measuring of direct-normal and/or diffuse irradiance adds an additional level of accuracy (Note: In the absence of the latter two parameters, models have to be used to split global irradiation into direct and diffuse).

The purpose of this work is to validate seven solar radiation models on tilted surfaces that are implemented in widely used building energy simulation codes including: EnergyPlus (2005), DOE-2.1E (2002), ESP-r (2005), and TRNSYS-TUD (2005). The seven models examined include:

- Isotropic sky (Hottel and Woertz, 1942 as cited by Duffie and Beckman, 1991).
- Klucher (1979).
- Hay and Davies (1980).
- Reindl (1990).
- Muneer (1997).
- Perez et al. (1987).
- Perez et al. (1990).

Two of three measured irradiance components were used in each simulation and predictions of global vertical irradiance on a façade oriented 29° West of South were compared with measurements. Particular emphasis was placed on quantifying how uncertainty in the input parameters-direct-normal, diffuse and horizontal global solar irradiance as well as ground reflectance and surface azimuth angle-propagated through radiation calculation algorithms and impacted the global vertical irradiance calculation. Sensitivity analyses were performed using both the Monte Carlo analysis (MCA) and fitted effects for N-way factorials.

2. Solar radiation models

Total solar irradiance on a tilted surface can be divided into two components: (1) the beam component from direct irradiation of the tilted surface and (2) the diffuse component. The sum of these components equates to the total irradiance on the tilted surface and is described in Eq. (1).

$$I_{\mathrm{T}} = I_{\mathrm{T,b}} + I_{\mathrm{T,d}} \tag{1}$$

Studies of clear skies have led to a description of the diffuse component being composed of an isotropic diffuse component $I_{\mathrm{T,d,iso}}$ (uniform irradiance from the sky dome), circumsolar diffuse component $I_{\mathrm{T,d,cs}}$ (resulting from the forward scattering of solar radiation and concentrated in an area close to the sun), horizon brightening component $I_{\mathrm{T,d,hb}}$ (concentrated in a band near the horizon and most pronounced in clear skies), and a reflected component that quantifies the radiation reflected from the ground to the tilted surface $I_{\mathrm{T,d,g}}$. A more complete version of Eq. (1) containing all diffuse components is given in Eq. (2).

$$I_{\mathrm{T}} = I_{\mathrm{T,b}} + I_{\mathrm{T,d,iso}} + I_{\mathrm{T,d,cs}} + I_{\mathrm{T,d,hb}} + I_{\mathrm{T,d,g}} \tag{2}$$

For a given location (longitude, latitude) at any given time of the year (date, time) the solar azimuth and altitude can be determined applying geometrical relationships. Therefore, the incidence angle of beam radiation on a tilted surface can be computed. The models described in this paper all handle beam radiation in this way so the major modeling differences are calculations of the diffuse radiation. An overview of solar radiation modeling used for thermal engineering is provided in numerous textbooks including Duffie and Beckman (1991) and Muneer (1997). Solar radiation models with different complexity which are widely implemented in building energy simulation codes will be briefly described in the following sections.

2.1. Isotropic sky model

The isotropic sky model (Hottel and Woertz, 1942 as cited by Duffie and Beckman, 1991; Liu and Jordan, 1960) is the simplest model that assumes all diffuse radiation is uniformly distributed over the sky dome and that reflection on the ground is diffuse. For surfaces tilted by an angle β from the horizontal plane, total solar irradiance can be written as shown in Eq. (3).

$$I_{\mathrm{T}} = I_{\mathrm{h,b}}R_{\mathrm{b}} + I_{\mathrm{h,d}}\left(\frac{1+\cos\beta}{2}\right) + I_{\mathrm{h}}\rho\left(\frac{1-\cos\beta}{2}\right) \tag{3}$$

Circumsolar and horizon brightening parts (Eq. (2)) are assumed to be zero.

2.2. Klucher model

Klucher (1979) found that the isotopic model gave good results for overcast skies but underestimates irradiance under clear and partly overcast conditions, when there is increased intensity near the horizon and in the circumsolar region of the sky. The model developed by Klucher gives the total irradiation on a tilted plane shown in Eq. (4).

$$I_{\mathrm{T}} = I_{\mathrm{h,b}}R_{\mathrm{b}} + I_{\mathrm{h,d}}\left(\frac{1+\cos\beta}{2}\right)\left[1+F'\sin^3\left(\frac{\beta}{2}\right)\right] \times [1+F'\cos^2\theta\sin^3\theta_{\mathrm{z}}] + I_{\mathrm{h}}\rho\left(\frac{1-\cos\beta}{2}\right) \tag{4}$$

F' is a clearness index given by Eq. (5).

$$F' = 1-\left(\frac{I_{\mathrm{h,d}}}{I_{\mathrm{h}}}\right)^2 \tag{5}$$

The first of the modifying factors in the sky diffuse component takes into account horizon brightening; the second takes into account the effect of circumsolar radiation. Under overcast skies, the clearness index F' becomes zero and the model reduces to the isotropic model.

2.3. Hay–Davies model

In the Hay–Davies model, diffuse radiation from the sky is composed of an isotropic and circumsolar component (Hay and Davies, 1980) and horizon brightening is not taken into account. The anisotropy index A defined in Eq. (6) represents the transmittance through atmosphere for beam radiation.

$$A = \frac{I_{\mathrm{bn}}}{I_{\mathrm{on}}} \tag{6}$$

The anisotropy index is used to quantify a portion of the diffuse radiation treated as circumsolar with the remaining portion of diffuse radiation assumed isotropic. The circumsolar component is assumed to be from the sun's position. The total irradiance is then computed in Eq. (7).

$$I_{\mathrm{T}} = (I_{\mathrm{h,b}} + I_{\mathrm{h,d}}A)R_{\mathrm{b}} + I_{\mathrm{h,d}}(1-A)\left(\frac{1+\cos\beta}{2}\right) + I_{\mathrm{h}}\rho\left(\frac{1-\cos\beta}{2}\right) \tag{7}$$

Reflection from the ground is dealt with like in the isotropic model.

2.4. Reindl model

In addition to isotropic diffuse and circumsolar radiation, the Reindl model also accounts for horizon brightening (Reindl et al., 1990a,b) and employs the same definition of the anisotropy index A as described in Eq. (6). The total irradiance on a tilted surface can then be calculated using Eq. (8).

$$I_{\mathrm{T}} = (I_{\mathrm{h,b}} + I_{\mathrm{h,d}}A)R_{\mathrm{b}} + I_{\mathrm{h,d}}(1-A)\left(\frac{1+\cos\beta}{2}\right) \times \left[1+\sqrt{\frac{I_{\mathrm{h,b}}}{I_{\mathrm{h}}}}\sin^3\left(\frac{\beta}{2}\right)\right] + I_{\mathrm{h}}\rho\left(\frac{1-\cos\beta}{2}\right) \tag{8}$$

Reflection on the ground is again dealt with like the isotropic model. Due to the additional term in Eq. (8) representing horizon brightening, the Reindl model provides slightly higher diffuse irradiances than the Hay–Davies model.

2.5. Muneer model

Muneer's model is summarized by Muneer (1997). In this model the shaded and sunlit surfaces are treated separately, as are overcast and non-overcast conditions of the sunlit surface. A tilt factor T_{F} representing the ratio of the slope background diffuse irradiance to the horizontal diffuse irradiance is calculated from Eq. (9).

$$T_{\mathrm{F}} = \left(\frac{1+\cos\beta}{2}\right) + \frac{2B}{\pi(3+2B)} \times \left[\sin\beta - \beta\cos\beta - \pi\sin^2\frac{\beta}{2}\right] \tag{9}$$

For surfaces in shade and sunlit surfaces under overcast sky conditions, the total radiation on a tilted plane is given in Eq. (10).

$$I_{\mathrm{T}} = I_{\mathrm{h,b}}R_{\mathrm{b}} + I_{\mathrm{h,d}}T_{\mathrm{F}} + I_{\mathrm{h}}\rho\left(\frac{1-\cos\beta}{2}\right) \tag{10}$$

Sunlit surfaces under non-overcast sky conditions can be calculated using Eq. (11).

$$I_{\mathrm{T}} = I_{\mathrm{h,b}}R_{\mathrm{b}} + I_{\mathrm{h,d}}[T_{\mathrm{F}}\ (1-A) + AR_{\mathrm{b}}] + I_{\mathrm{h}}\rho\left(\frac{1-\cos\beta}{2}\right) \tag{11}$$

The values of the radiation distribution index B depend on the particular sky and azimuthal conditions, and the location. For European locations, Muneer recommends fixed values for the cases of shaded surfaces and sun-facing surfaces under an overcast sky, and a function of the anisotropic index for non-overcast skies.

2.6. Perez model

Compared with the other models described, the Perez model is more computationally intensive and represents a more detailed analysis of the isotropic diffuse, circumsolar and horizon brightening radiation by using empirically derived coefficients (Perez et al., 1990). The total irradiance on a tilted surface is given by Eq. (12).

$$I_T = I_{h,b}R_b + I_{h,d}\left[(1-F_1)\left(\frac{1+\cos\beta}{2}\right) + F_1\frac{a}{b} + F_2\sin\beta\right] + I_h\rho\left(\frac{1-\cos\beta}{2}\right) \quad (12)$$

Here, F_1 and F_2 are circumsolar and horizon brightness coefficients, respectively, and a and b are terms that take the incidence angle of the sun on the considered slope into account. The terms a and b are computed using Eqs. (13) and (14), respectively.

$$a = \max(0^\circ, \cos\theta) \quad (13)$$

$$b = \max(\cos 85^\circ, \cos\theta_z) \quad (14)$$

The brightness coefficients F_1 and F_2 depend on the sky condition parameters clearness ε and brightness Δ. These factors are defined in Eqs. (15) and (16), respectively.

$$\varepsilon = \frac{\frac{I_{h,d}+I_n}{I_{h,d}} + 5.535\cdot 10^{-6}\theta_z^3}{1 + 5.535\cdot 10^{-6}\theta_z^3} \quad (15)$$

$$\Delta = m\frac{I_{h,d}}{I_{on}} \quad (16)$$

F_1 and F_2 are then computed in Eqs. (17) and (18), respectively.

$$F_1 = \max\left[0, \left(f_{11} + f_{12}\Delta + \frac{\pi\theta_z}{180}f_{13}\right)\right] \quad (17)$$

$$F_2 = f_{21} + f_{22}\Delta + \frac{\pi\theta_z}{180}f_{23} \quad (18)$$

The coefficients $f_{11}, f_{12}, f_{13}, f_{21}, f_{22}$, and f_{23} were derived based on a statistical analysis of empirical data for specific locations. Two different sets of coefficients were derived for this model (Perez et al., 1990; Perez et al., 1987).

3. Facility and measurements

3.1. Test site and setup

The solar radiation measurements were performed on the EMPA campus located in Duebendorf, Switzerland (Longitude 8°36′55″ East, Latitude 47°24′12″ North at an elevation of 430 m above sea level). Fig. 1 shows the facility which was designed to measure solar gains of transparent façade components; a detailed description of the facility is provided by Manz et al. (in press). For this study, only the pyranometers and the pyrheliometer at the facility were used (Figs. 1 and 2). For the diffuse measurements, a shading disk was mounted in front of the pyranometer with the same solid angle as the pyrheliometer that blocked out the beam irradiance component (Fig. 2). In order to evaluate the robustness of various radiation models, two 25 day periods were studied to compare predicted irradiance on the tilted façade with measured data that were recorded by a pyranometer mounted on the vertical surface (29° West of South) of the test cell. The dates of the first and second periods were October 2 to October 26, 2004 and March 22 to April 16, 2005, respectively. Both periods include a range of different atmospheric conditions and solar positions. The solar radiation data were acquired for 600 h for each period.

Fig. 1. Test cells with pyranometers visible in the central part of the picture and green artificial turf installed in front of the test cell.

Fig. 2. Pyrheliometer for measuring direct-normal and shaded pyranometer for measuring diffuse horizontal solar irradiance are positioned on the roof of the facility.

3.2. Solar irradiance

Table 1 indicates measured parameters, type of instrument used and accuracies of sensors specified by the manufacturers. To verify the accuracy of the instrumentation, the global horizontal irradiance can be calculated using solar position and direct-normal and horizontal diffuse irradiance shown in Eq. (19).

$$I_h = I_{b,n}\sin\alpha_s + I_{h,d} \quad (19)$$

The differences between global horizontal irradiance measured and computed based on direct-normal (beam) and horizontal diffuse irradiance were analyzed. Using the experimental uncertainties described in Table 1, 95% credible limits were calculated for the measured global horizontal irradiance using manufacturer's error and for the computed global irradiance using propagation of error

Table 1
Instruments used for measuring solar irradiance

Parameter	Unit	Type of sensor/measurement	Number of sensors	Accuracy
Solar global irradiance, façade plane (29° W of S)	W/m^2	Pyranometer (Kipp & Zonen CM 21)	1	± 2% of reading
Solar global horizontal irradiance	W/m^2	Pyranometer (Kipp & Zonen CM 21)	1	± 2% of reading
Solar diffuse horizontal irradiance	W/m^2	Pyranometer, mounted under the shading disc of a tracker (Kipp & Zonen CM 11)	1	± 3% of reading
Direct-normal irradiance	W/m^2	Pyrheliometer, mounted in an automatic sun-following tracker(Kipp & Zonen CH 1)	1	± 2% of reading

techniques (uncertainty analysis) assuming uniform distributions (Glesner, 1998). From these comparisons, the 95% credible limits from the calculated and measured global horizontal irradiance for Periods 1 and 2 were found to overlap 78.0% and 70.1% of the time, respectively; these calculations were only performed when the sun was up ($\alpha_s > 0$). Careful examination of these results reveals that the discrepancies occurred when the solar altitude angles and irradiance were small or the solar irradiance were very large (especially for Period 2). Linear regression analysis was used to compare the computed global irradiance using measured beam and diffuse irradiances and measured global irradiances. The results from this analysis are shown for Periods 1 and 2 in Figs. 3a and 3b, respectively. The differences between calculated and measured quantities are apparent from the slopes of lines. These results reveal a slight systematic under-prediction by roughly 3% of global horizontal irradiance when calculating it from the beam and diffuse horizontal irradiance components.

3.3. Ground reflectance

The importance of accurately quantifying the albedo in lieu of relying on default values is discussed in detail by Ineichen et al. (1987). Therefore, in order to have a well-defined and uniform ground reflectance, artificial green turf was installed in front of the test cell to represent a typical outdoor surface (Fig. 1).

Reflectance of a sample of the artificial turf was measured at almost perpendicular (3°) incident radiation in the wavelength interval between 250 nm and 2500 nm using an integrating sphere (Fig. 4) which could not be employed

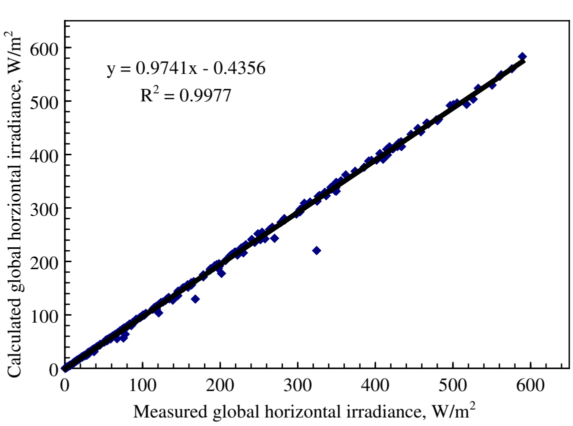

Fig. 3a. Measured and calculated global horizontal irradiance for Period 1.

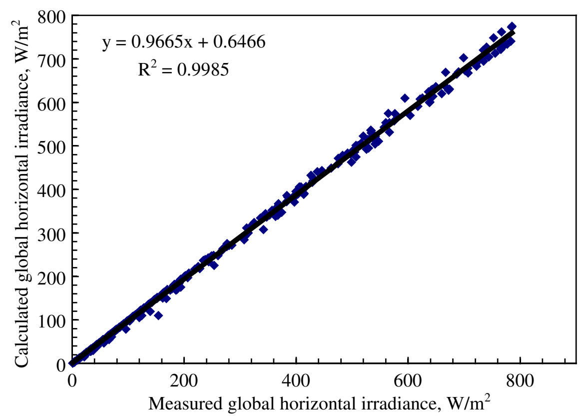

Fig. 3b. Measured and calculated global horizontal irradiance for Period 2.

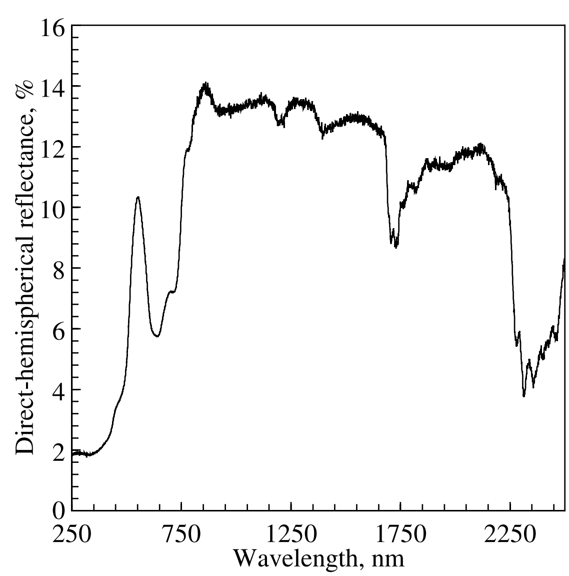

Fig. 4. Near direct normal-hemispherical reflectance of the artificial turf.

for angular dependent measurements. Specular components of the reflectance were measured at incident angles of 20°, 40°, and 60° and were found to be less than 1%; therefore the surface was considered to be a Lambertian surface (Modest, 2003). Integral values for reflectance were determined according to European Standard EN 410 (1998) by means of GLAD Software (2002). Hemispherical–hemispherical reflectance was then determined at each wavelength assuming an angular dependent surface absorptance as shown in Eq. (20) (from Duffie and Beckman, 1991).

$$\frac{\alpha(\theta)}{\alpha_n} = \begin{cases} 1 + 2.0345\times10^{-3}\theta - 1.99\times10^{-4}\theta^2 + 5.324\times10^{-6}\theta^3 - 4.799\times10^{-8}\theta^4 & 0^\circ \leqslant \theta \leqslant 80^\circ \\ -0.064\theta + 5.76 & 80^\circ \leqslant \theta \leqslant 90^\circ \end{cases} \tag{20}$$

Eq. (21) was used to calculate the hemispherical–hemispherical reflectance.

$$\rho = 2\int_{0^\circ}^{90^\circ} (1-\alpha(\theta))\sin(\theta)\cos(\theta)\,\mathrm{d}\theta \tag{21}$$

This integral was evaluated numerically using the Engineering Equation Solver (Klein, 2004). The computed solar ground reflectance shown in Table 2a corresponds well with albedo measurements described by Ineichen et al. (1987) in Table 2b.

4. Simulations

The incident (global vertical) irradiance on the exterior façade for all the building energy simulation codes was a function of the solar irradiance and ground reflectance. Four building energy simulation codes: EnergyPlus, DOE-2.1e, ESP-r and TRNSYS-TUD, which encompassed seven different radiation models that were evaluated for both periods.

EnergyPlus version 1.2.2 uses the 1990 Perez model. For the simulation, measured direct-normal and diffuse horizontal solar irradiance were used as inputs in 10 min and six timesteps each hour. DOE-2.1e also uses a Perez 1990 model to calculate irradiance on a tilted façade (Buhl, 2005) with hourly inputs of direct-normal and global horizontal solar irradiance. Both EnergyPlus and DOE-2.1e assumed a constant annual direct-normal extraterrestrial irradiation term (they do not factor in the elliptical orbit of the earth around the sun). TRNSYS-TUD allows the user to select from four models and various inputs for solar irradiance. For these experiments, the Isotropic, Hay–Davies, Reindl, and Perez 1990 model were used with inputs of measured direct normal and global horizontal irradiance; the inputs to the models were in 1 h timesteps. The extraterrestrial irradiation was varied to account for the elliptical orbit of the sun for the Perez, Reindl, and Hay–Davies models. ESP-r has the Perez 1990 model as its default, but other models are available to the user, namely the Isotropic, Klucher, Muneer and Perez 1987 models. Measured 6 min averaged data were input to the program. The program also takes into account variations in the extraterrestrial radiation in the Perez and Muneer models. It is also possible to use direct-normal plus diffuse horizontal irradiances, or global horizontal plus diffuse horizontal irradiances as inputs to ESP-r; for this study, only the direct normal and diffuse horizontal inputs were used.

Table 2a
Solar ground reflectance

Parameter	Reflectance, %
Hemispherical–hemispherical	14.8 ± 0.74
Near direct normal-hemispherical	8.8

Table 2b
Ineichen et al. (1987) measurements for determining average albedo coefficients over a three-month period

Parameter	Reflectance, %				
	Horizontal	North	East	South	West
Horizontal	13.4	–	–	–	–
Differentiated		14.7	15.5	13.8	14.8
Morning		13.9	14.3	14.3	15.7
Afternoon		16.0	17.2	13.1	13.5

5. Sensitivity analysis

Sensitivity studies are an important component in thorough empirical validations; such studies were therefore also performed. The uncertainties in the input parameters were taken from information provided by the manufacturers (Table 1). The error in the ground reflectance calculation (models and measurements combined) was estimated as 5% (see Table 2) and ±1° for the building azimuth. Uniform distributions were assumed for estimated uncertainties and quantities provided by manufacturers (Glesner, 1998). Although all the codes perform solar angle calculations, uncertainties were not assigned to the test cell locations (latitude, longitude, and elevation). Two types of sensitivity analysis were performed for this project in EnergyPlus which included fitted effects for N-way factorials and MCA. For these analyses the source code was not modified, but rather a "wrap" was designed to modify input parameters in the weather file and the input file for EnergyPlus in MatLab Version 7.0.0.19920 (2004). A Visual Basic program was written to create a command line executable program to run the "WeatherConverter" program and the "RunEplus.bat" program was run from the

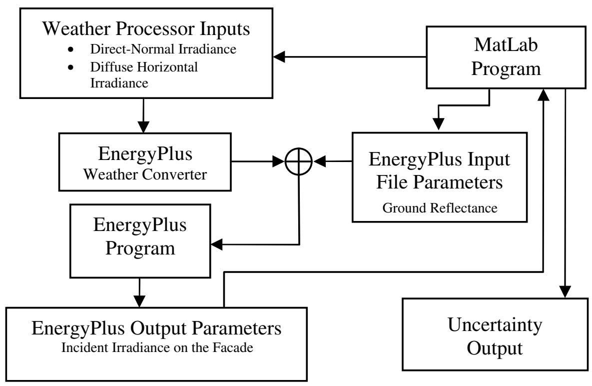

Fig. 5. Flowchart for the sensitivity studies.

MatLab program. Output from each run was recorded in output files. A flowchart for this process is depicted in Fig. 5.

5.1. Fitted effects for N-way factorials

A fitted effects N-way factorial method was used to identify the impact of uncertainties in various parameters on the results (Vardeman and Jobe, 2001). The parameters that were varied for this study included: ground reflectance, building azimuth, direct-normal irradiance, global horizontal irradiance (which was an unused parameter in EnergyPlus), and diffuse irradiance. Therefore, for this study a fitted effects for a Three-way factorial analysis was performed. The first step in this process is to run a one-way factorial shown in Eq. (22) varying each parameter. This equation is equivalent to the commonly used differential sensitivity analysis.

$$u_i = \phi(\xi_i + \sigma_i) - \phi(\xi_i) \tag{22}$$

For uniform distributions, the standard deviation is estimated in Eq. (23).

$$\sigma_i = \frac{d}{\sqrt{3}} \tag{23}$$

The two-way factorials were estimated using Eq. (24). Additional levels of interactions were considered but were found to be negligible.

$$u_{ij} = \phi(\xi_i + \sigma_i, \xi_j + \sigma_j) - (\phi(\xi_i, \xi_j) + u_i + u_j) \quad i \neq j \tag{24}$$

The overall uncertainty was estimated using the quadrature summation shown in Eq. (25).

$$u = \sqrt{\sum u_i^2 + \sum u_{ij}^2} \tag{25}$$

This analysis assumes a localized linear relationship where the function is evaluated. To confirm this assumption, estimates were made by forward differencing ($\xi_i + \sigma_i$) and backward differencing ($\xi_i - \sigma_i$). The individual factorials can also be analyzed to assess their impact. In Table 3, the results from this analysis averaged over the entire test ($\alpha_s > 0$) are shown for both forward and backward differencing. Looking at the results from forward and backward difference, the assumed localized linear relationship seems reasonable but may lead to minor discrepancies that are discussed later.

5.2. Monte Carlo analysis

The Monte Carlo method can be used to analyze the impact of all uncertainties simultaneously by randomly varying the main input parameters and performing multiple evaluations of the output parameter(s). When setting up the analysis, the inputs are modified according to a probability density function (pdf) and, after numerous iterations, the outputs are assumed to be Gaussian (normal) by the Central Limit Theorem. The error is estimated by taking the standard deviation of the multiple evaluations at each time step. MatLab 7.0 can be used to generate random numbers according to Gaussian, uniform, and many other distributions. A comprehensive description and the underlying theory behind the Monte Carlo Method are provided by Fishman (1996) and Rubinstein (1981).

5.2.1. Sampling

For this study, Latin hypercube sampling was used. In this method, the range of each input factor is divided into

Table 3
Average factorial impacts ($\alpha_s > 0$)

Factorial	Period 1		Period 2	
	Forward differencing, W/m^2	Backward differencing, W/m^2	Forward differencing, W/m^2	Backward differencing, W/m^2
I_{bn}	1.13	−1.10	1.23	−1.31
$I_{h,d}$	1.37	−1.28	1.50	−1.59
ρ	0.357	−0.357	0.566	−0.566
ϕ_b	−0.499	0.500	−0.291	0.303
$I_{bn} \times I_{h,d}$	−0.05596	−0.0831	0.0663	0.0531
$I_{bn} \times \rho$	0.00155	0.00158	0.00308	0.00310
$I_{bn} \times \phi_b$	−0.00464	−0.00464	−0.0027	−0.00274
$I_{h,d} \times \rho$	0.00352	0.00380	0.00514	0.00516
$I_{h,d} \times \phi_b$	−0.00267	−0.00264	−0.00094	−0.000907
$\rho \times \phi_b$	No interactions	No interactions	No interactions	No interactions
u	2.40	2.40	2.85	2.95

equal probability intervals based on the number of runs of the simulation; one value is then taken from each interval. When applying this method for this study given parameters with non-uniform distributions, the intervals were defined using the cumulative distribution function and then one value was selected from each interval assuming a uniform distribution (again this was simplified in using MatLab because the functions were part of the code). This method of sampling is better when a few components of input dominate the output (Saltelli et al., 2000). For this study, the input parameters were all sampled from a uniform distribution. Previous studies have shown that after 60–80 runs there are only slight gains in accuracy (Fürbringer and Roulet, 1995), but 120 runs were used to determine uncertainty. The average overall uncertainties ($\alpha_s > 0$) for Periods 1 and 2 were 2.35 W/m^2 and 2.87 W/m^2, respectively; the results corresponded well with the fitted effects model. The results at any given time step are discussed in the next Section (5.3).

5.2.2. Analysis of output

It can be shown that despite the pdf's for input parameters, the output parameters will always have a Gaussian distribution (given a large enough sample and sufficient number of inputs) by the Central Limit Theorem; therefore a Lilliefore Test for goodness of fit to normal distribution was used to test significance at 5% (when $\alpha_s > 0$). Using this criterion, 27.5% and 11.5% of the outputs from Periods 1 and 2, respectively, were found not to be normally distributed. A careful study of these results reveals that the majority of these discrepancies occurred when the direct-normal irradiance is small or zero. This may be due to the proportional nature of the uncertainties used for these calculations. At low direct-normal irradiances, the calculation becomes a function of only three inputs rather than four, which could make the pdf for the output parameter more susceptible to the individual pdf's of the input parameters, which for these cases were uniform distributions.

5.3. Estimated uncertainties

Estimates for uncertainties were obtained from both fitted effects for *N*-way factorial and MCA. From these analyses, both methods yield similar results. The only discrepancies for both forward and backward differencing were that fitted effects estimates are sometimes overestimated at several individual timesteps. Careful inspection of the individual responses revealed that there was a significant jump in the two-way direct-normal/diffuse response (sometimes in the order of 5 W/m^2) that corresponds to odd behavior in the one-way responses. The response for the rest of the timesteps was negligible. Additional review showed that these events do not occur during the same timesteps for forward and backward differencing. It was therefore assumed that these discrepancies result from localized non-linearities at these timesteps.

6. Results

The computed results from the four simulation codes were compared with the measured global vertical irradiance. Comparisons were made using the nomenclature and methodology proposed by Manz et al. (in press). An important term used for comparing the performance of the respective models in the codes is the uncertainty ratio. This term was computed at each hour ($\alpha_s > 0$) and is shown in Eq. (26). The average, maximum, and minimum quantities are summarized in the statistical analyses for each test. Ninety-five percent credible limits were calculated from the MCA for EnergyPlus and the 95% credible limits for the experiment were estimated assuming a uniform distribution. The credible limits from EnergyPlus were used to calculate the uncertainty ratios for all the models and codes. For the uncertainty ratio, terms less than unity indicate that the codes were validated with 95% credible limits.

$$\mathrm{UR} = \frac{|D|}{\mathrm{OU}_{\mathrm{Experiment}} + \mathrm{OU}_{\mathrm{EnergyPlus}}} \tag{26}$$

Tables 4–6 show the results from Periods 1 and 2 and combined periods, respectively. Plots were constructed that depict the global vertical irradiation (hourly averaged irradiance values multiplied by a 1 h interval) and credible limits. For these plots, the output and 95% credible limits for a given hour of the day were averaged to provide an overview of the performance of each model. Figs. 6–8 contain results from Periods 1 and 2 and the combined results.

7. Discussion and conclusions

The accuracy of the individual radiation models and their implementation in each building energy simulation code for both periods can be accurately assessed from the statistical analyses and the plots from the results section. Fig. 6 shows that in the morning, there are both over and under-prediction of the global vertical irradiance by the models for Period 1; in the afternoon the global vertical irradiance is significantly under-predicted by most models. During Period 2, the majority of the models over-predict the global vertical irradiance for most hours during the day. Combining these results helps to redistribute the hourly over and under-predictions from each model, but it is still clear when comparing the uncertainty ratios that all the models performed better during Period 1.

Using the average uncertainty ratio as a guide, it can be seen that for both periods none of the models were within overlapping 95% credible limits. Strictly speaking, none of the models can therefore be considered to be validated within the defined credible limits ($\overline{\mathrm{UR}} > 1$). This is partly due to the proportional nature of the error which at vertical irradiance predictions with small uncertainties leads to large hourly uncertainty ratio calculations and the difficulty in deriving a generic radiation model for every location in the world. This is also shown in Figs. 6–8 where

Table 4
Analysis of global vertical façade irradiance in W/m^2 ($\alpha_s > 0$) for Period 1

	Experiment	EnergyPlus Perez 1990	DOE-2.1e Perez 1990	TRNSYS-TUD Hay–Davies	TRNSYS-TUD Isotropic	TRNSYS-TUD Reindl	TRNSYS-TUD Perez 1990	ESP-r Perez 1990	ESP-r Perez 1987	ESP-r Klucher	ESP-r Isotropic	ESP-r Muneer
$\bar{x}$	176.1	169.7	177.2	165.1	157.8	170.9	169.8	188.2	192.8	174.8	171.9	191.4
s	223.8	211.8	218.6	205.1	190.1	209.4	211.1	218.2	220.5	196.9	192.5	226.3
x_{max}	856.8	817.8	820.4	801.2	743.2	810.4	796.4	804.7	806.7	743.5	728.8	915.7
x_{min}	0.2	0.3	0.0	0.4	0.9	0.4	0.3	0.2	0.1	0.3	0.3	0.2
$\overline{D}$	–	−6.4	1.1	−11.0	−18.3	−5.2	−6.3	1.9	6.6	−11.5	−14.3	5.1
$\overline{\lvert D\rvert}$	–	13.7	10.5	18.0	26.2	15.7	11.7	13.3	14.7	24.6	27.8	14.1
D_{max}	–	103.5	67.1	108.0	138.9	90.4	73.3	87.7	86.7	139.1	157.7	205.5
D_{min}	–	0.0	0.0	0.0	0.0	0.0	0.0	0.0	0.0	0.0	0.0	0.0
D_{rms}	–	24.2	17.0	28.9	44.4	24.0	21.0	21.4	22.1	39.1	44.7	24.6
$D_{95\%}$	–	56.4	40.3	71.7	111.2	56.3	57.1	50.9	51.5	96.5	110.7	53.3
$\overline{OU}$	6.90	4.62	–	–	–	–	–	–	–	–	–	–
$\overline{UR}$	–	1.34	1.34	2.28	4.03	2.29	1.12	1.43	1.69	2.50	2.63	1.54
UR_{max}	–	12.42	20.41	20.41	129.05	20.41	10.20	11.22	12.09	17.04	17.04	13.48
UR_{min}	–	0.00	0.01	0.00	0.00	0.00	0.00	0.00	0.00	0.01	0.00	0.00
$\overline{\lvert D\rvert}/\bar{x}$	–	7.8	5.9	10.2	14.9	8.9	6.7	6.7	6.7	14.8	16.7	7.2
$\overline{D}/\bar{x}$	–	−3.7	0.6	−6.2	−10.4	−3.0	−3.6	−2.7	−0.1	−11.3	−13.4	1.0

Table 5
Analysis of global vertical façade irradiance in W/m^2 ($\alpha_s > 0$) for Period 2

	Experiment	EnergyPlus Perez 1990	DOE-2.1e Perez 1990	TRNSYS-TUD Hay–Davies	TRNSYS-TUD Isotropic	TRNSYS-TUD Reindl	TRNSYS-TUD Perez 1990	ESP-r Perez 1990	ESP-r Perez 1987	ESP-r Klucher	ESP-r Isotropic	ESP-r Muneer
$\bar{x}$	194.5	208.5	210.5	199.7	191.6	207.7	201.4	202.0	206.7	190.1	187.9	202.5
s	222.1	226.3	231.3	219.0	201.5	224.1	225.2	222.4	223.8	201.3	197.3	224.2
x_{max}	797.1	796.3	828.5	807.8	741.4	820.2	801.7	794.6	799.5	730.4	720.2	801.1
x_{min}	0.3	0.3	0.0	0.4	0.4	0.4	0.3	0.2	0.2	0.3	0.3	0.2
$\overline{D}$	–	14.0	16.0	5.2	−2.9	13.2	6.9	7.5	12.2	−4.4	−6.6	8.0
$\overline{\lvert D\rvert}$	–	19.4	17.6	16.2	25.0	19.0	12.7	14.6	17.2	23.4	26.4	15.4
D_{max}	–	104.0	77.3	59.5	122.6	67.2	63.5	81.3	86.7	113.0	134.9	86.9
D_{min}	–	0.0	0.1	0.1	0.1	0.1	0.0	0.0	0.0	0.0	0.0	0.0
D_{rms}	–	29.2	26.3	20.9	35.2	24.5	19.2	22.2	24.5	33.6	38.8	24.0
$D_{95\%}$	–	70.1	62.4	42.6	81.7	51.1	46.3	50.9	58.0	79.9	93.2	55.6
$\overline{OU}$	7.62	5.62	–	–	–	–	–	–	–	–	–	–
$\overline{UR}$	–	2.11	2.12	2.66	3.06	2.99	1.41	1.61	2.00	2.60	2.73	1.64
UR_{max}	–	12.83	21.70	20.62	20.63	21.41	11.21	9.70	11.24	14.94	14.94	13.48
UR_{min}	–	0.00	0.02	0.01	0.03	0.01	0.01	0.00	0.00	0.01	0.01	0.00
$\overline{\lvert D\rvert}/\bar{x}$	–	10.0	9.1	8.3	12.9	9.8	6.5	7.5	8.8	12.0	13.6	7.9
$\overline{D}/\bar{x}$	–	7.2	8.2	2.7	−1.5	6.8	3.5	3.9	6.3	−2.3	−3.4	4.1

Table 6
Analysis of global vertical façade irradiance in W/m^2 ($\alpha_s > 0$) for both periods

	Experiment	EnergyPlus Perez 1990	DOE-2.1e Perez 1990	TRNSYS-TUD Hay–Davies	TRNSYS-TUD Isotropic	TRNSYS-TUD Reindl	TRNSYS-TUD Perez 1990	ESP-r Perez 1990	ESP-r Perez 1987	ESP-r Klucher	ESP-r Isotropic	ESP-r Muneer
$\bar{x}$	186.2	191.0	195.5	184.1	176.3	191.1	187.1	188.2	192.8	174.8	171.9	191.4
s	222.9	220.6	226.1	213.4	197.0	218.2	219.4	218.2	220.5	196.9	192.5	226.3
$x_{\max}$	856.8	817.8	828.5	807.8	743.2	820.2	801.7	804.7	806.7	743.5	728.8	915.7
$x_{\min}$	0.2	0.3	0.0	0.4	0.4	0.4	0.3	0.2	0.1	0.3	0.3	0.2
$\overline{D}$	–	4.8	9.3	−2.1	−9.9	4.9	0.9	1.9	6.6	−11.5	−14.3	5.1
$\overline{\lvert D\rvert}$	–	16.8	14.4	17.0	25.6	17.5	12.2	13.3	14.7	24.6	27.8	14.1
$D_{\max}$	–	104.0	77.3	108.0	138.9	90.4	73.3	87.7	86.7	139.1	157.7	205.5
$D_{\min}$	–	0.0	0.0	0.0	0.0	0.0	0.0	0.0	0.0	0.0	0.0	0.0
D_{rms}	–	27.1	22.6	24.8	39.6	24.3	20.0	21.4	22.1	39.1	44.7	24.6
$D_{95\%}$	–	65.7	55.1	54.9	99.4	54.2	48.7	50.9	51.5	96.5	110.7	53.3
$\overline{\text{OU}}$	7.30	4.46	–	–	–	–	–	–	–	–	–	–
$\overline{\text{UR}}$	–	1.91	1.90	2.57	3.61	2.77	1.38	1.43	1.69	2.50	2.63	1.54
$\text{UR}_{\max}$	–	17.62	29.31	28.31	129.05	29.39	15.38	11.22	12.09	17.04	17.04	13.48
$\text{UR}_{\min}$	–	0.00	0.01	0.00	0.00	0.00	0.00	0.00	0.00	0.01	0.00	0.00
$\overline{\lvert D\rvert}/\bar{x}$	–	9.0	7.7	9.1	13.7	9.4	6.6	7.2	7.9	13.2	14.9	7.6
$\overline{D}/\bar{x}$	–	2.6	5.0	−1.1	−5.3	2.6	0.5	1.0	3.5	−6.2	−7.7	2.8

there is very little overlap in the experimental and MCA 95% credible limits. But the average uncertainty ratio can also be used as a guide to rank the overall performance of the tilted radiation models. The Isotropic model performed the worst during these experiments, which can be expected because it was the most simplistic and did not account for the various individual components of diffuse irradiance. While the Reindl and Hay–Davies model accounted for the additional components of diffuse irradiance (both circumsolar and horizontal brightening for the Reindl and circumsolar for the Hay–Davies), the Perez formulation – which relied on empirical data to quantify the diffuse components – provided the best results for this location and wall orientation. Differences between the Perez models in the four building energy simulation codes can be attributed to solar irradiance input parameters (beam, global horizontal, and diffuse), timesteps of the weather measurements, solar angle algorithms, and assumptions made by the programmers (constant direct-normal extraterrestrial radiations for DOE-2.1e and EnergyPlus). For both periods, the assumptions made in the TRNSYS-TUD formulation Perez radiation model performed best. But also from these results, the Muneer model performed quite well without the detail used in the Perez models. In fact, the Muneer model performed better than Perez models formulated in EnergyPlus and DOE-2.1e.

The presented results reveal distinct differences between radiation models that will ultimately manifest themselves in the solar gain calculations. Mean absolute deviations in predicting solar irradiance for both time periods were: (1) 13.7% and 14.9% for the isotropic sky model, (2) 9.1% for the Hay–Davies, (3) 9.4 % for the Reindl, (4) 7.6% for the Muneer model, (5) 13.2% for the Klucher, (6) 9.0%, 7.7%, 6.6%, and 7.1% for the 1990 Perez, and (7) 7.9% for the 1987 Perez models. This parameter is a good estimate of the instantaneous error that would impact peak load calculations. The mean deviations calculations for these time periods were: (1) −5.3% and −7.7% for the isotropic sky model, (2) −1.1% for the Hay–Davies, (3) 2.6% for the Reindl, (4) 2.8% for the Muneer model, (5) −6.2% for the Klucher, (6) 2.6%, 5.0%, 0.5%, and 1.0% for the 1990 Perez, and (7) 3.5% for the 1987 Perez models. From this parameter it can be concluded that building energy simulation codes with advanced radiation models are capable of computing total irradiated solar energy on building façades with a high precision for longer time periods (such as months). Hence, the calculations of building energy consumption with high prediction accuracy is achievable even in today's highly glazed buildings, which are largely affected by solar gains. On the other hand, even the most advanced models deviate significantly at specific hourly timesteps (up to roughly 100 W/m^2), which poses serious limitations to accuracy of predictions of cooling power at a specific point in time, the short-time temperature fluctuations in the case of non-air conditioned buildings or the control and/or sizing of HVAC equipment or shading devices. When performing building simulations, engineers

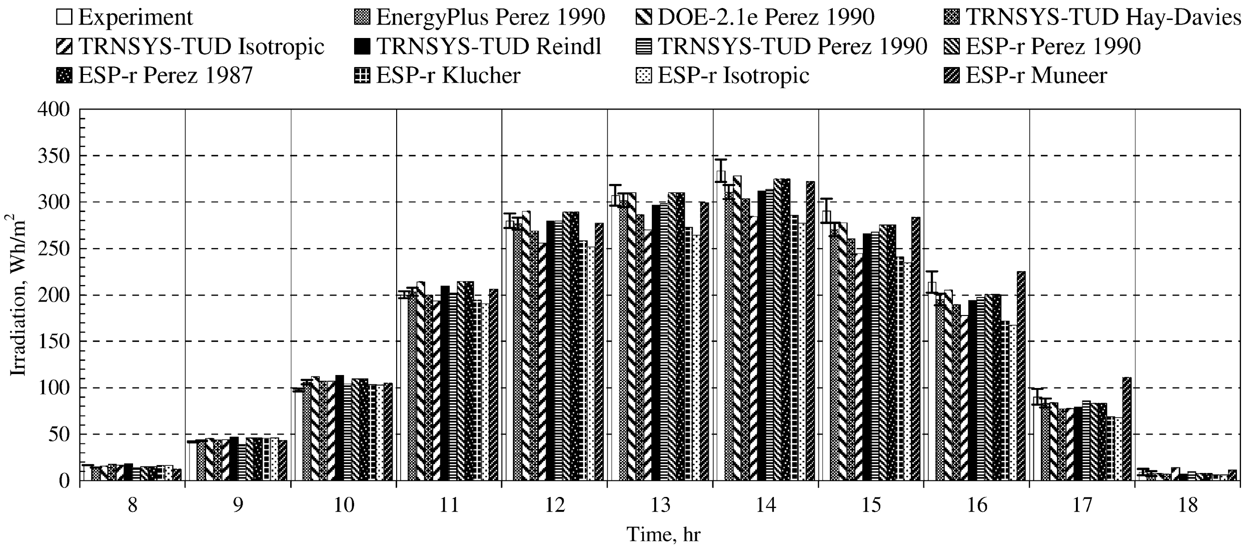

Fig. 6. Average hourly irradiation comparisons for the vertical façade for Period 1.

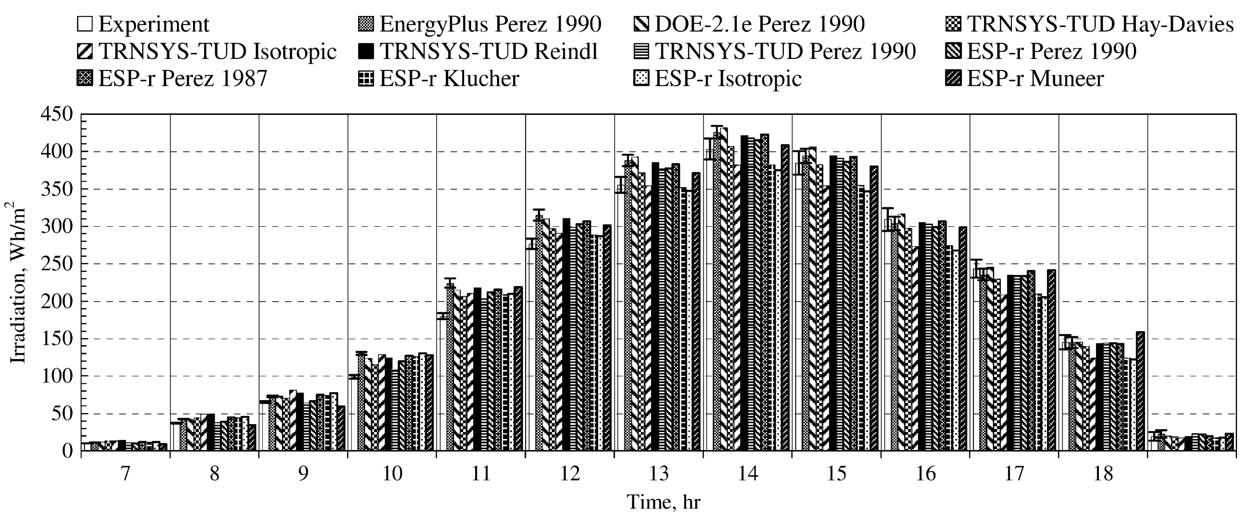

Fig. 7. Average hourly irradiation comparisons for the vertical façade for Period 2.

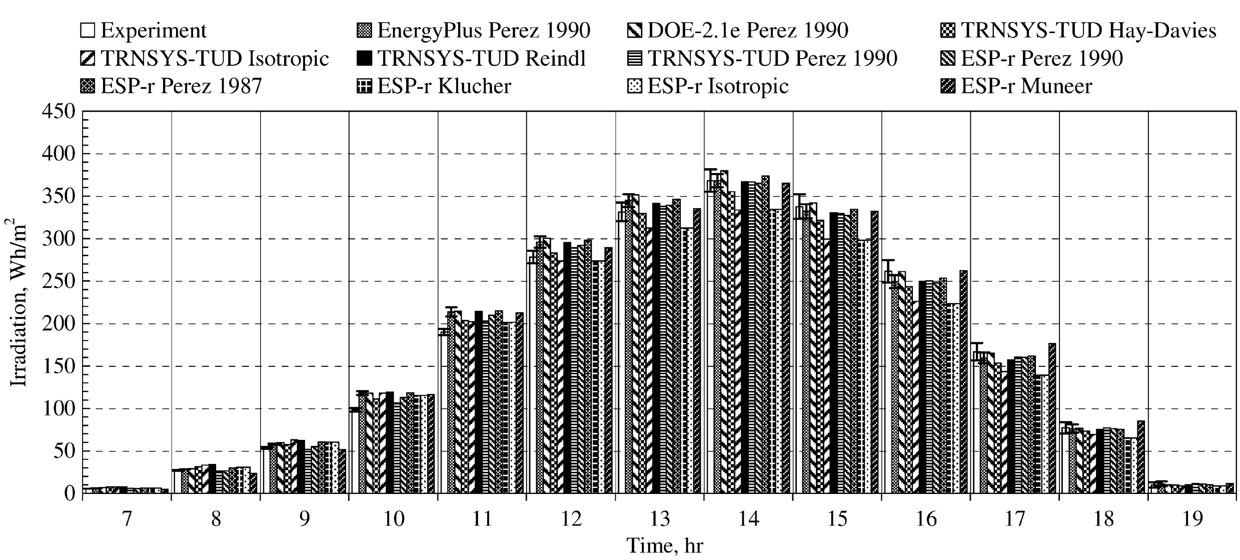

Fig. 8. Average hourly irradiation comparisons for the vertical façade combining both periods.

must consider much higher uncertainties at specific timesteps.

Additional factors that were not investigated include the number of components of solar irradiance measured at a given weather station (often only global horizontal irradiance is measured and other models are used to compute beam irradiance), locations and densities of the weather stations used as inputs for building simulation codes, and reliability of weather files used by building energy simulation codes. While this study is somewhat limited to a specific location and time period, it reveals the importance of making proper assessments concerning tilted radiation models and their implementations in building energy simulation codes.

Note: Radiation data and data of all other experiments within the IEA Task 34 project can be downloaded from our website at www.empa.ch/ieatask34.

Acknowledgements

We gratefully acknowledge with thanks the financial support from the Swiss Federal Office of Energy (BFE) for building and testing the experimental facility (Project 17′166) as well as the funding for EMPA participation in IEA Task 34/43 (Project 100′765). We would also like to acknowledge Dr. M. Morris from the Iowa State University Statistics Department for his clear direction with regard to formulating the sensitivity analysis and the many contributions from our colleagues R. Blessing, S. Carl, M. Camenzind, and R. Vonbank.

References

Aude, P., Tabary, L., Depecker, P., 2000. Sensitivity analysis and validation of buildings' thermal models using adjoint-code method. Energy and Buildings 30, 267–283.

Badescu, V., 2002. 3D isotropic approximation for solar diffuse irradiance on tilted surfaces. Renewable Energy 26, 221–233.

Behr, H.D., 1997. Solar radiation on tilted south oriented surfaces: validation of transfer-models. Solar Energy 61 (6), 399–413.

Buhl, F., 2005. Private email correspondence exchanged on March 9, 2005 with Peter Loutzenhiser at EMPA that contained the radiation model portion of the DOE-2.1E source code, Lawrence Berkley National Laboratories (LBNL).

DOE-2.1E, (Version-119). 2002. Building Energy Simulation Code, (LBNL), Berkley, CA, April 9, 2002.

Duffie, J.A., Beckman, W.A., 1991. Solar Engineering of Thermal Processes, Second ed. John Wiley & Sons, New York, Chichester, Brisbane, Toronto, Singapore.

EnergyPlus Version, 1.2.2.030. 2005. Building Energy simulation code. Available from: <www.energyplus.gov>.

ESP-r, Version 10.12, 2005. University of Strathclyde. Available from: <www.esru.strath.ac.uk>.

European Standard EN 410, 1998. Glass in building – determination of luminous and solar characteristics of glazing. European Committee for Standardization, Brussels, Belgium.

Fishman, G.S., 1996. Monte Carlo: Concepts, Algorithms, and Applications. Springer, New York Berlin Heidelberg.

Fürbringer, J.M., Roulet, C.A., 1995. Comparison and combination of factorial and Monte-Carlo design in sensitivity analysis. Building and Environment 30 (4), 505–519.

Fürbringer, J.M., Roulet, C.A., 1999. Confidence of simulation results: put a sensitivity analysis module in you MODEL: the IEA-ECBCS Annex 23 experience of model evaluation. Energy and Buildings 30, 61–71.

GLAD Software, 2002. Swiss Federal Laboratories for Materials Testing and Research (EMPA), Duebendorf, Switzerland.

Glesner, J.L., 1998. Assessing uncertainty in measurement. Statistical Science 13 (3), 277–290.

Gueymard, C., 1987. An anisotropic solar irradiance model for tilted surfaces and its comparison with selected engineering algorithms. Solar Energy 38 (5), 367–386.

Hay, J.E., Davies, J.A., 1980. Calculations of the solar radiation incident on an inclined surface. In: Hay, J.E., Won, T.K. (Eds.), Proc. of First Canadian Solar Radiation Data Workshop, 59. Ministry of Supply and Services, Canada.

Hottel, H.C., Woertz, B.B., 1942. Evaluation of flat-plate solar heat collector. Trans. ASME 64, 91.

Ineichen, P., Perez, R., Seals, R., 1987. The importance of correct albeto determination for adequately modeling energy received by a tilted surface. Solar Energy 39 (4), 301–305.

Klein, S.A., 2004. Engineering Equation Solver (EES) Software, Department of Mechanical Engineering. University of Wisconsin, Madison.

Klucher, T.M., 1979. Evaluation of models to predict insolation on tilted surfaces. Solar Energy 23 (2), 111–114.

Li, D.H.W., Lam, J.C., Lau, C.C.S., 2002. A new approach for predicting vertical global solar irradiance. Renewable Energy 25, 591–606.

Liu, B.Y.H., Jordan, R.C., 1960. The interrelationship and characteristic distribution of direct, diffuse, and total solar radiation. Solar Energy 4 (3), 1–19.

Lomas, K.J., Eppel, H., 1992. Sensitivity analysis techniques for building thermal simulation programs. Energy and Buildings 19, 21–44.

Macdonald, I., Strachan, P., 2001. Practical applications of uncertainty analysis. Energy and Buildings 33, 219–227.

Manz, H., Loutzenhiser, P., Frank, T., Strachan, P.A., Bundi, R., and Maxwell, G., in press. Series of experiments for empirical validation of solar gain modeling in building energy simulation codes – Experimental setup, test cell characterization, specifications and uncertainty analysis. Building and Environment.

Mara, T.A., Garde, F., Boyer, H., Mamode, M., 2001. Empirical validation of the thermal model of a passive solar test cell. Energy and Buildings 33, 589–599.

MatLab Version 7.0.0.19920, 2004. The MathWorks Inc.

Modest, M., 2003. Radiative Heat Transfer, Second ed. Academic Press, Amsterdam.

Muneer, T., 1997. Solar Radiation and Daylight Models for the Energy Efficient Design of Buildings. Architectural Press, Oxford.

Olmo, F.J., Vida, J., Castro-Diez, Y., Alados-Arboledas, L., 1999. Prediction of global irradiance on inclined surfaces from horizontal global irradiance. Energy 24, 689–704.

Palomo del Barrio, E., Guyon, G., 2003. Theoretical basis for empirical model validation using parameter space analysis tools. Energy and Buildings 35, 985–996.

Palomo del Barrio, E., Guyon, G., 2004. Application of parameters space analysis tools fro empirical model validation. Energy and Buildings 36, 23–33.

Perez, R., Stewart, R., Arbogast, C., Seals, R., Scott, J., 1986. An anisotropic hourly diffuse radiation model for sloping surfaces: Description, performanace validation, site dependency evaluation. Solar Energy 36 (6), 481–497.

Perez, R., Seals, R., Ineichen, P., Stewart, R., Menicucci, D., 1987. A new simplified version of the Perez diffuse irradiance model for tilted surfaces. Solar Energy 39 (3), 221–232.

Perez, R., Ineichen, P., Seals, R., Michalsky, J., Stewart, R., 1990. Modeling daylight availability and irradiance components from direct and global irradiance. Solar Energy 44 (5), 271–289.

Reindl, D.T., Beckmann, W.A., Duffie, J.A., 1990a. Diffuse fraction correlations. Solar Energy 45 (1), 1–7.

Reindl, D.T., Beckmann, W.A., Duffie, J.A., 1990b. Evaluation of hourly tilted surface radiation models. Solar Energy 45 (1), 9–17.
Remund, J., Salvisberg, E., Kunz, S., 1998. On the generation of hourly shortwave radiation data on tilted surfaces. Solar Energy 62 (5), 331–334.
Robledo, L., Soler, A., 2002. A simple clear skies model for the luminous efficacy of diffuse solar radiation on inclined surfaces. Renewable Energy 26, 169–176.
Rubinstein, R.Y., 1981. Simulation and the Monte Carlo Method. John Wiley & Sons, New York, Chichester, Brisbane, Toronto.
Saltelli, A., Chan, K., Scott, E.M., 2000. Sensitivity Analysis. John Wiley & Sons, Ltd, Chichester, New York, Weinheim, Brisbane, Singapore, Toronto.
Saltelli, A., Tarantola, S., Campolongo, F., Ratto, M., 2004. Sensitivity Analysis in Practice: A Guide to Assessing Scientific Models. John Wiley & Sons, LTD.
Santner, T.J., Williams, B.J., Notz, W.I., 2003. The Design and Analysis of Computer Experiments. Springer, New York, Berlin, Heidelberg.
TRNSYS-TUD, 2005. Technical University of Dresden research code based on the frame of TRNSYS 14.2, Solar Energy Laboratory, University of Wisconsin-Madison, Madison, WI, 1996.
Vardeman, S.B., Jobe, J.M., 2001. Data Collection and Analysis. Duxbury Thomson Learning, Australia, Canada, Mexico, Singapore, Spain, United Kingdom, United States.